

Laser Deposition of (Cu + Mo) Alloying Reinforcements on AA1200 Substrate for Corrosion Improvement.

A.P.I. Popoola^{1,*}, S.L. Pityana^{1,2} and O.M. Popoola¹

¹ Faculty of Engineering and the Built Environment, Tshwane University of Technology, P.M.B X680, Pretoria, South Africa, 0001.

² Center for Scientific and Industrial Research – National Laser Centre, P.O. Box 395, BLD 46F, Pretoria, South Africa, 0001.

*E-mail: PopoolaAPI@tut.ac.za

Received: 17 August 2011 / Accepted: 15 September 2011 / Published: 1 October 2011

Poor corrosion performance of aluminium alloys in marine environment has been a subject of intensive research recently. Aluminium substrate was alloyed with a combination of two metallic powders (Cu + Mo) using an Nd: YAG solid state laser. Solidification of the laser induced melt pool led to the precipitation of different intermetallic compounds. Characterisation of the resultant microstructure was carried out by optical and scanning electron microscopes. X-ray diffraction and energy dispersive spectrometry was used for phase and elemental composition analyses respectively. Experimental results showed that the microstructure of the alloyed zone consisted of a continuous network of Al₂Cu precipitates which is the initial phase at the background enveloping the Al-matrix, on top of the initial phase are the Al₅Mo intermetallic precipitates and eutectics of (α -Al + Al₂Cu) and (α -Al + Al₅Mo). The addition of 50%Cu and 50%Mo to the Al solid solution increased the electrode potential; decreased the anodic activation; promoted the formation of stable passivation on the surface of aluminium and greatly decreased corrosion reactions. A significant increase in the corrosion resistance of the aluminium was achieved as a result of laser surface alloying.

Keywords: Intermetallics, Laser alloyed layer, Corrosion, Passivity, Anodic reaction

1. INTRODUCTION

Aluminium alloys are important materials for the technological development of the world. Aluminium alloys are one of the most commonly utilized materials in composite fabrication and this is attributed to their desirable chemical, physical and mechanical properties. Aluminium-based intermetallic composites containing reinforced hard particles offer superior operating performance and resistance to wear and corrosion [a-d]. The resulting high specific properties can provide significant

weight savings in many components compared with conventional aluminium alloys. Aluminium (Al) exhibit poor surface properties because of its low melting point and weak interatomic bonds [a-d].

Corrosion is one of the surface dependent properties of metallic materials. It is the destruction of metals by electrochemical/chemical agencies. It is an interfacial process occurring on the surface of metallic materials when exposed to different environments, chemicals and etc. [e-i].

The corrosion process takes place at the metal-medium phase boundary, therefore it is an heterogeneous reaction in which the structure and condition of the metal's surface have a significant role. Aluminium alloys do not corrode when exposed to air, this is because Al has a high affinity for oxygen and it does form a protective oxide film of $\text{Al}_2\text{O}_3 \cdot n\text{H}_2\text{O}$ on its surface; this effectively protects it in air. However, when aluminium alloys are used in marine environment they severely corrode, the halide ion penetrates the oxide film and severe pitting corrosion takes place leading to the formation of complex Al salt.

Laser surface alloying (LSA) is an advanced processing technology that has potential to deposit various metallic and ceramic powdery materials locally on surfaces. Reports indicated that it can be used to improve corrosion, wear and other surface related properties of components. The surface layers produced by this process differ from those produced by numerous deposition techniques in that there is no discontinuity in the chemical and mechanical properties at the coating-substrate interface. The alloyed layer microstructure so evolved is a function of the laser processing parameters and its chemical composition, and this finally determines the mechanism of corrosion and hence the degree of enhancement obtained [a-i].

In the current investigation, the alloying powders used were copper (Cu) and molybdenum (Mo). It has been reported that when copper is added to Al alloys it brings about an improvement in mechanical properties. Mo can withstand extreme temperatures without significantly expanding or softening and as such it is very useful in applications that involve high temperatures. It is also a metal that exhibit high corrosion resistance hence its usage in the manufacture of some stainless steels. Molybdenum acts by increasing the lattice strain, thus increasing the energy required to dissolve out, meaning dissolution is very hard to achieve with Mo.

Many investigations have been carried out in this regard: Man et al. (2001) carried out laser surface alloying of Al6061 with NiCrSiB powder mixed with a binding agent using a high power Nd: YAG laser. Good metallurgical bonding was evident in alloyed layers and consists of intermetallic phases of NiAl, Ni_3Al , NiAl_3 , and Al_3Ni_2 in the form of fine dendritic structures. The pitting potential for both the alloyed layer and the as-received specimens is approximately the same. Passivation was not observed in the laser-alloyed layer. The protection potential of the alloyed layer is shifted to the noble direction when compared with the as-received. The enhancement of the corrosion potential was achieved. The cavitation erosion resistance of the laser-alloyed surface is 100% better than that of the Al6061 alloy [a]. Almeida et al. (1995) states that alloyed layers can be produced in substrates of aluminium and 7175 high resistance alloy by laser melting with injection of chromium powder. The size and the concentration of chromium powder particles determine the result obtained from surface alloying. The corrosion resistance of 7175 alloy and aluminium is enhanced after LSA with chromium due to the formation of a passive film containing chromium oxide, which delays stable pitting initiation [b]. In this paper Watkins et al. (1998) reports the characteristics and corrosion behaviour of

the overlapped areas in the laser melting and alloying with Cr, W, Zr-Ni or Ti-Ni of 2014 aluminium alloy. The as-received 2014 alloys surfaces displayed pitting resistances lower than that of Al-Cr alloyed surfaces alloyed with CO₂ laser. A selective dissolution at interface dominated the corrosion performance for W alloyed surfaces, but for the other three alloys (Cr, Zr-Ni or Ti-Ni in aluminium) this phenomenon was less pronounced [c].

Xu, Yue and Man (2008) pointed out that interdendritic boundaries are vulnerable to corrosion attacks due to the presence of second phase particles. That preferential dissolution of dendrite cores generally occurred in the Nd: YAG laser-treated specimens, in which most of the second particles behaved as cathodic sites and dendrite cells as anodic sites. The authors carried out laser surface treatment of aluminium alloy 6013 with the objective of improving the alloy's resistance to pitting corrosion fatigue. The study showed that laser melting using a high power Nd: YAG laser increased the resistance of the alloy to pitting corrosion and pitting corrosion fatigue [d].

The present study aims at improving the corrosion properties of pure Al by laser surface alloying technique. The fabrication of Al/(Cu + Mo) intermetallic matrix composites will be carried out. The laser processing parameters will be optimized. Investigation of the influences of Cu and Mo combined reinforcements on the microstructure and corrosion properties of aluminium AA1200 will also be undertaken.

2. MATERIALS AND METHODS

Commercially pure Aluminium AA1200 was the subject of study. The material was cut and machined to dimensions 100 x 100 x 6 mm. To boost the laser energy absorption at the surface of the substrate, sand blasting was done to achieve a uniform rough and clean surface.

Laser surface alloying of the substrate was then carried out using a Rofin Sinar continuous wave Nd: YAG solid-state laser. The Nd: YAG laser is fitted with off-axes nozzle used for powder feeding. The shielding gas used was argon, this prevent oxidation during the alloying process. The process was then optimized by continuously running a series of tests. Single tracklines were made on the substrate, the optimized laser parameters for the aluminium alloyed surface is laser power 4 kW, laser alloying speed 1.5 m/min, powder feed rate 4 g/min and beam diameter 3 mm.

2.1. Materials characterization

Following laser irradiation, a detailed characterization of the alloyed layer was undertaken in terms of microstructure, composition and phases. Chemical reactions between molten aluminium and the metallic alloying powders led to the precipitation of different intermetallic compounds within the matrix.

The new phases formed were studied. Cutting, grinding and polishing of alloyed layers were carried out. The polished surfaces were etched using Keller's reagent. The new phases were characterized by optical and scanning electron microscopes while energy dispersive spectroscopy EDS

was used for the constituent elements identification. The characteristics of the phases were studied by means of X-ray diffraction, a Philips PW 1713 diffractometer fitted with a monochromatic Cu K α radiation set at 40 kV and 20 mA was used to determine the phase composition of substrate and alloyed layers. The scan was taken between 10° and 80° two theta (2 Θ) with a step size of 0.02 degree. Phase identification was done using Philips Analytical X'Pert HighScore® software with an in-built International Centre for Diffraction Data (ICSD) database.

2.2. Electrochemical test

A linear potentiodynamic polarization test and open circuit corrosion potential measurements were carried out on the alloyed sample and the as-received sample. Measurements were done using an Autolab potentiostat (PGSTAT30 computer controlled) with the General Purpose Electrochemical Software (GPES) package version 4.9. Measurements were made at room temperature using 3.65% NaCl solution.

The solution for this study was prepared from analytical grade reagents and distilled water. An electrochemical cell consisting of working electrode (samples) graphite rods as the counter electrodes and a silver/silver chloride 3 M KCl electrode as the reference electrode (SCE). The specimens were mounted in epoxy resin, and ground down to 1200 grit silicon carbide paper prior to measurements. The corrosion potential (E_{corr}), and corrosion rate were determined accordingly. The specimen were scanned from a potential of -1.51 V with respect to stabilized open circuit potential (E_{ocp}) at a rate of 0.25 mV s⁻¹. All the potentials reported were versus the SCE potentials.

3. RESULT AND DISCUSSIONS

3.1. Characterization of the substrate

The chemical composition of the substrate can be seen in Table 1. From this Table, AA1200 contains over 99% of Al, and as such the substrate can be regarded as pure Al.

Table 1. Chemical composition of the substrate material

Element	Al	Fe	Cu	Si
Composition (wt.%)	Balance	0.59	0.12	0.13

Figure 1 is the x-ray diffractograph of pure Al. From the spectrum, peaks of Al and Fe can be seen. Fe has the highest wt. % after Al itself in this material.

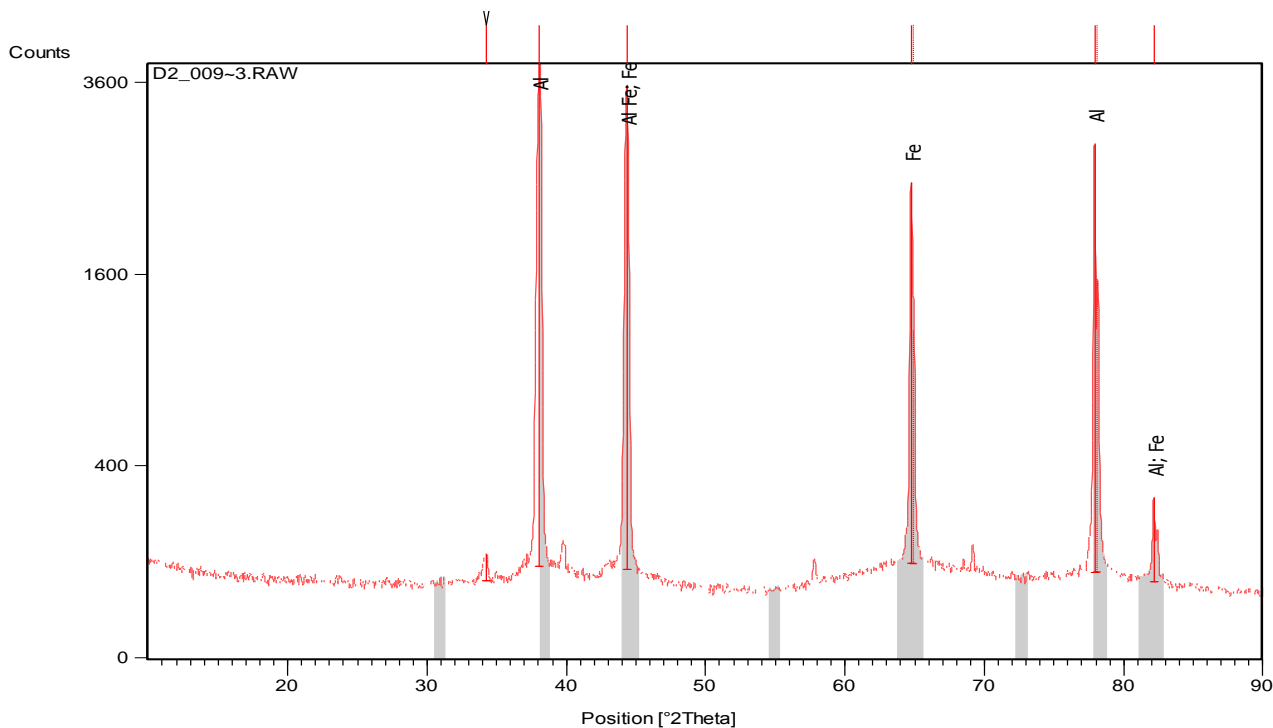


Figure 1. X-ray diffractogram of aluminium AA1200

The surface morphology of the substrate material can be seen in Figure 2.

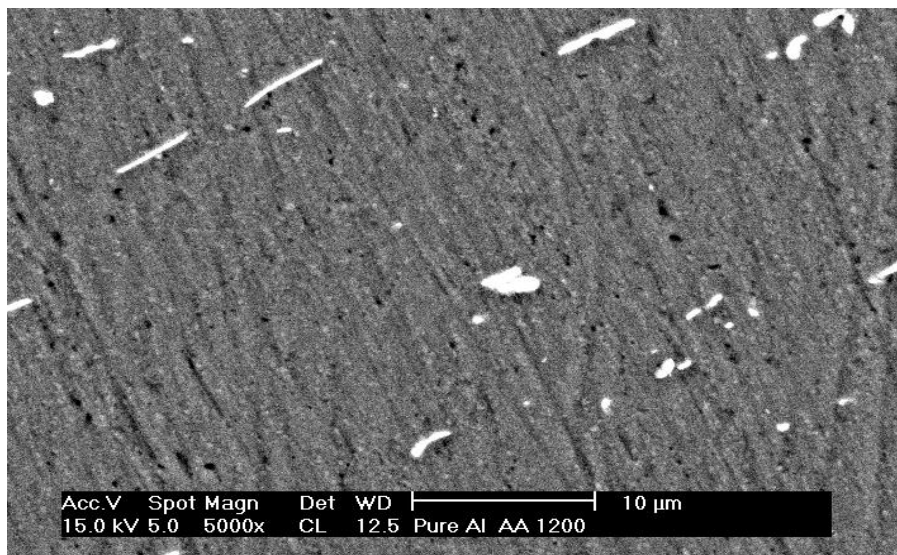


Figure 2. SEM spectrum of aluminium AA1200

3.2.Characterization of microstructure of alloyed layer

Laser irradiation caused convective flow within the melt pool which was intensive enough to

solidification rate hence the growth of primary phases (heterogeneous phases) was limited as a result of fast cooling rate.

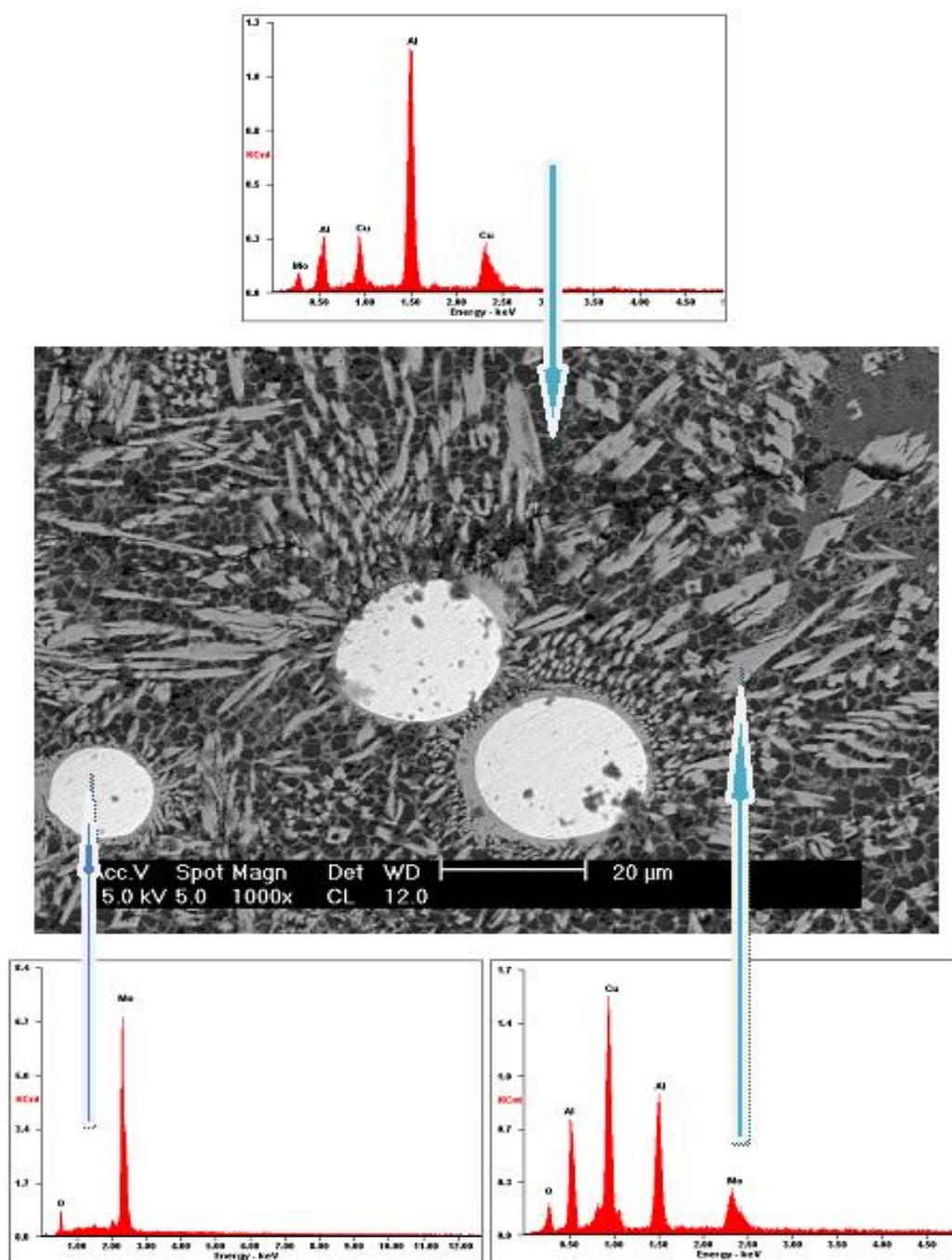


Figure 4. SEM/EDS spectra of Al-Cu-Mo alloyed layer

3.3. Electrochemical test result

Potentiostatic polarization can be used to calculate the electrochemical parameters. Figure 5 shows a cyclic polarization curves for Al-Cu-Mo alloyed layer and the as-received Al in a 3.65 wt. %

NaCl solution. Table 2 list the corrosion potential (E_{corr}), corrosion current density (I_{corr}) and all results derived from polarization curves.

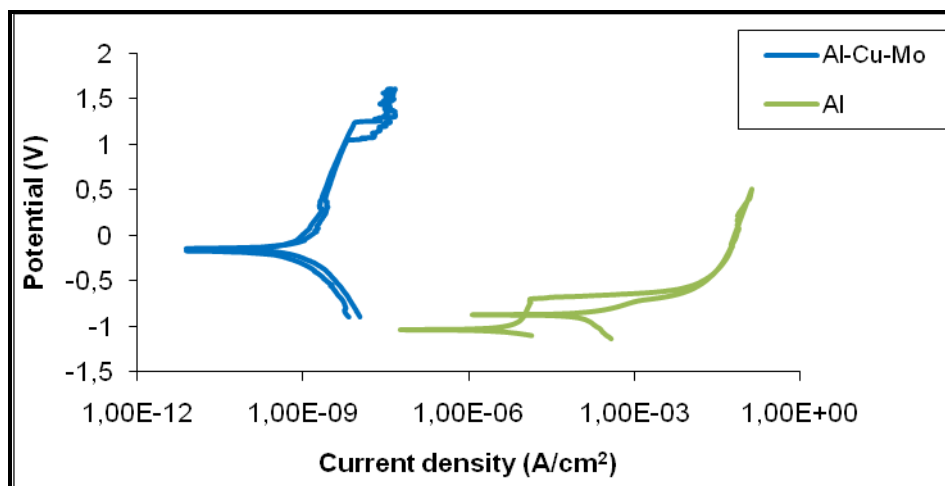


Figure 5. Cyclic polarisation curves of the alloyed sample Al-Cu-Mo sample and the as-received Al

Table 2. Polarization Data

Alloy type	E_{corr} (V)	I_{corr} (A/cm ²)	i_{corr} (A)	E_{pit} (V)	R_p (Ω)	β_a (V/dec)	β_c (V/dec)	Corrosion rate (mm/yr)
Al-Cu-Mo	-0.175	7.6×10^{-12}	9.9×10^{-13}	0.948	6.2×10^6	0.013	0.008	2.9×10^{-7}
AA1200	-1.036	2.3×10^{-6}	1.5×10^{-6}	-0.724	2.6×10^3	0.072	0.128	3.7×10^{-2}

The forward scan represents the polarization behaviour of the alloyed layer. On the forward scan, the corrosion potential of the alloyed sample is -0.175 V while that of as-received Al is -1.036 V. The corrosion potential was increased by 0.861 V because of the precipitation of Al_2Cu and Al_5Mo within the alloyed surface. Thus an increase in E_{corr} was achieved as a result of laser surface alloying. This suggests that the Al-Cu-Mo sample is much less active than the pure Al sample but not necessarily confirming the resistance of Al-Cu-Mo sample in the tested solution. On the reverse scan, the corrosion potential -0.245 V was recorded for alloyed sample and that of as-received Al was -0.871 V. The reverse scan is related to the corroded areas. The corrosion potential of the alloyed sample on the reverse scan also shifted to more positive values compared to that of Al sample, an increase of E_{corr} in the range of 0.626 V. The size between the forward and reverse scans before their intercession is the loop size, the corrosion protection E_{prot} determines the loop size. The smaller the loop size, the less the tendency of the material to pit. E_{prot} for the alloyed and as-received samples are -0.512 V and -0.9 V respectively, this value for the alloyed sample is more positive which then means that the tendency for the alloyed sample to pit is far less. This implies that the Al-Cu-Mo alloy fabricated through LSA technique has high corrosion resistance.

According to electrochemical principles, the corrosion rate is proportional to the corrosion current density; and reduced rate in corrosion current density will enhance passivity of the sample.

Definitely, a reduction in corrosion current density was achieved; from the forward scan, the I_{corr} of the alloyed sample and the as-received recorded are 7.6×10^{-12} and $2.3 \times 10^{-6} \text{ A/cm}^2$ respectively; a six order decrease in magnitude was achieved. On the reverse scan however, the I_{corr} are 1.25×10^{-11} and $1.16 \times 10^{-6} \text{ A/cm}^2$ for the alloyed and as-received samples, for both scans a reduction in corrosion current density was achieved.

The corrosion rate was also marginally reduced for the alloyed sample compared with the as-received sample (2.9×10^{-7} and $3.7 \times 10^{-2} \text{ mm/yr}$ respectively), a five-fold decrease was achieved as a result of deposition of *Mo* and *Cu* elements into Al-matrix.

According to Princeton applied research group, the materials with the highest polarization resistance R_p and the lowest corrosion current i_{corr} have the highest corrosion resistance compared to the other materials [m]. The R_p and i_{corr} for both the alloyed and the as-received samples are 6.2×10^6 & $2.6 \times 10^3 \Omega$: three orders magnitude increase and 6.8×10^{-12} & $1.5 \times 10^{-6} \text{ A}$: six orders magnitude decrease respectively. From this principle, the alloyed sample is more corrosion resistance.

There is significant change in pitting potential for the laser-alloyed specimen. The pitting potential E_{pit} for Al is -0.724 V and for the alloyed sample it is 0.948 V indicating an achievement of a huge increase in the pitting potential. The difference in the E_{pit} and E_{prot} parameters of a material is a measure of the extent of passivation range in pitting polarization curve. The $(E_{pit}-E_{prot})$ parameters for these samples are 0.176 V for Al and for Al-Cu-Mo alloy 1.46 V . It measures the susceptibility of a material to pitting corrosion. The larger the value of this parameter, the more resistant is the material to pitting corrosion. Looking at these values, the alloyed sample has better corrosion resistance. The repassivation power of the laser-treated sample is also very much higher than the as-received sample as shown by the value $(E_{pit}-E_{prot})$ for this sample.

Figure 6 shows the pit morphology of the as-received Al. In contact with air, aluminium alloys are covered with a film that contains aluminium oxide Al_2O_3 , $n\text{H}_2\text{O}$. Hence there is a pre-existing film on the surface of aluminium.

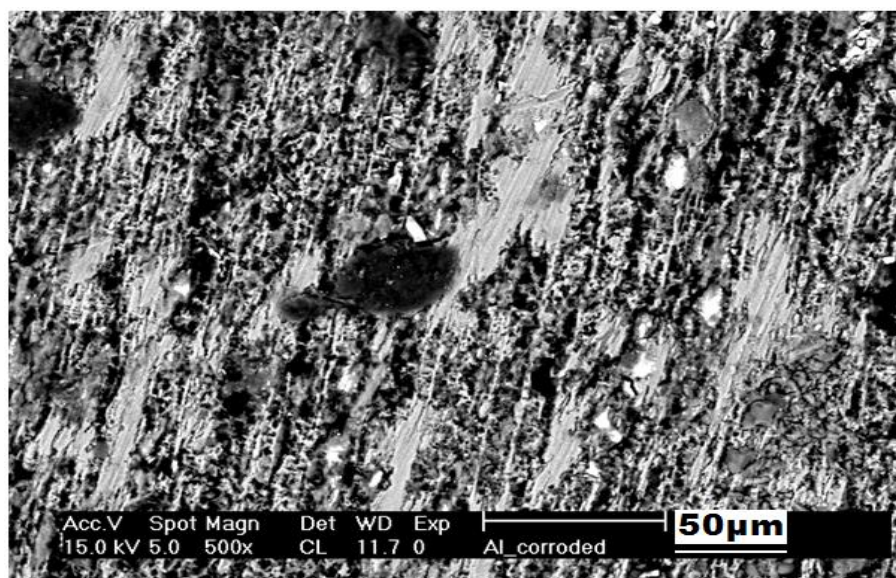
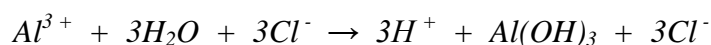


Figure 6. The SEM micrograph of pure Al substrate after corrosion test.

As the potential of the as-received Al is made more positive (anodic direction), the passive current density remains constant until such time the current begins to increase with potential. This indicates local breakdown of the pre-existing protective oxide film by the anions, which is followed by the halide ion penetrating the oxide solution interface of the as-received sample and severely attacking it. This led to the Cl^- being adsorbed on the oxide film ($Al_2O_3 \cdot nH_2O$ sites). Dissolution of the film occurs especially at weak points leading to exposure of the underlying metal which dissolves, giving rise to an increase in the anodic current with consequent formation of Al^{3+} (anodic oxidation reaction). The Al^{3+} undergoes hydrolysis thereby lowering the pH of the local solution. The pH of this solution attained a critical value which corresponds to the breakdown of the passive film, and then propagation of the corrosion attack took place. The oxide film is thinned to the extent that aluminium ions can pass from the metal to the solution interface. The chloride ion then reacts with the aluminium hydroxide formed or simply the aluminium ion produced from the anodic reaction of metal dissolution to produce hydroxychloride aluminium salt or simply aluminium chloride, resulting into propagation of severe pitting corrosion. The following reactions occur when the AA1200 is immersed in $NaCl$ solution.



Corrosion is usually accompanied by the formation of solid corrosion products from the reaction between the anodic and cathodic products, these reactions leads to the formation of metal hydroxides:



The high current associated with the dissociation reaction causes a migration of Cl^- into the broken down areas, where they tend to form chloride salts of the metals:



From Figure 6, it is evident that the as-received sample undergoes severe pitting corrosion. In this regard the alloyed sample exhibited good resistance to corrosion; therefore the presence of solute elements that makes film breakdown more difficult lowered the susceptibility of the alloy to pitting corrosion. The shift of the corrosion potential in the positive direction accompanied by an obvious decrease of the anodic current density suggests that such an aluminium-alloyed coating provides a typical anodic control protection. In general, the higher the value of the breakdown potential, the more resistant is the metal to pitting attack.

Passivity is a condition existing on a metal surface, because of the presence of a protective film that markedly lowers the rate of corrosion. From Figure 5, the range of passivation of the laser treated sample is wider than that of the untreated sample. This is in-line with the increased E_{pit} values recorded for this sample. Chloride ions are harmful to passivity. It is generally accepted that they have an important effect on the breakdown of the passive films and, consequently on pit initiation. When the film is locally broken down by these ions, local cells tend to develop which can have catastrophic effect. Some regions of the metal that became active will work as the anode whereas the larger regions of passive metal will work as cathode. The effect of the chlorides ions can be explained by their incorporation into the oxide films and by the ability of Cl^- to adsorb on the metal surface at sites where the oxide film has natural defects.

For the coatings investigated; the alloys react thus:

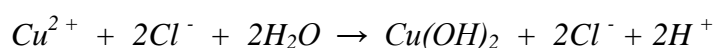


Figure 7 is the typical SEM micrograph of the microstructure of *Al-Cu-Mo* sample after exposure in 3.65 % *NaCl* solution. Severe pitting or localized corrosion was not seen on the surface of the laser treated sample but rather scales of corrosion products were observed. There is grey bead-like morphology as well as dark morphology on the sample. Elemental composition indicated the presence of *C*, *O*₂, *Na*, *Cl*, *Al*, *Mo* and *Cu* in the bead-like morphology. The SEM/EDS for laser alloyed sample shows the presence of carbon and oxides of *Al*, *Mo*, and *Cu*.

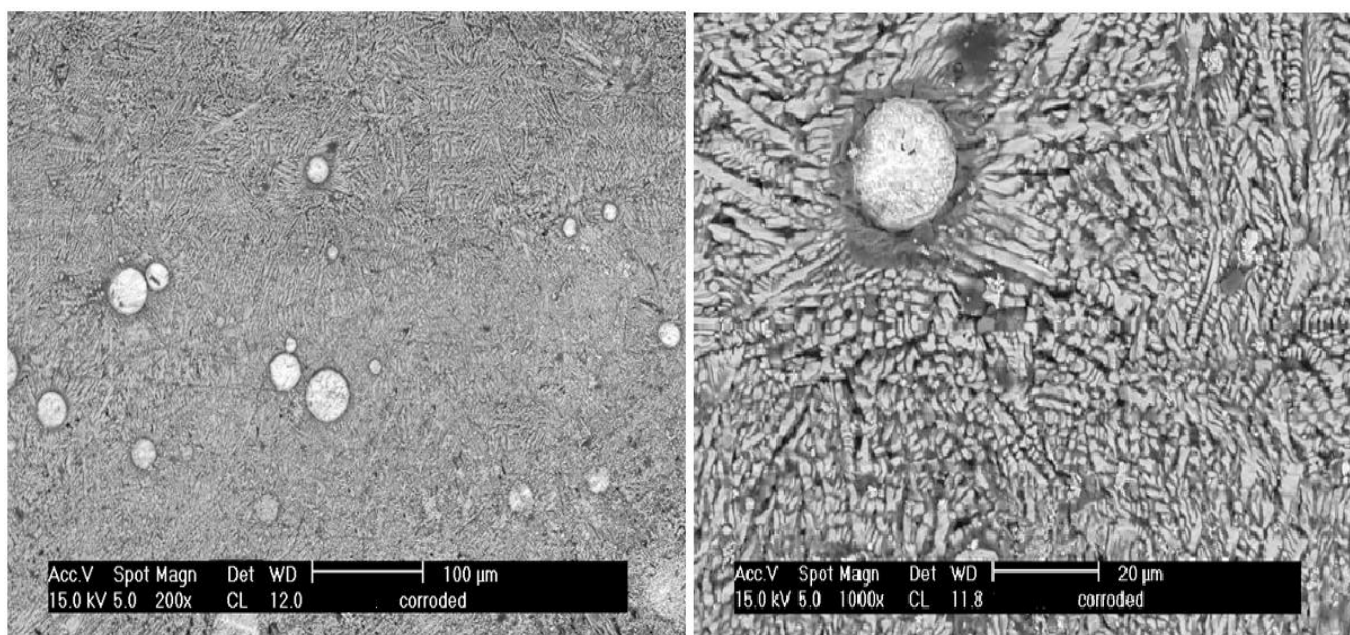


Figure 7. The SEM micrographs of the alloyed surface at high and low magnification after corrosion test

Laser processing limitations in LSA fabrications are usually microstructural inhomogeneity, segregation of alloying elements especially at reinforcement/matrix interfaces, pores, cracks and holes in the alloyed layers. Reports indicated that these limitations are responsible for increased corrosion attack in alloys fabricated even much more than the unreinforced alloys. In this study, investigations revealed slight degree of microstructural inhomogeneities in the sample alloyed as a result of the LSA process; this can be attributed to the convective flow of the molten liquid. Differences in mixing between the alloying elements and the molten substrate might have occurred and led to the microstructural inhomogeneities. The variation in their densities and thermo-physical properties (especially their melting temperature- *Mo* is a refractory metal having extremely high melting point) may also have resulted into inhomogeneity in microstructure of the intermetallic composite. Uniform and complete mixing in the liquid pool is a prime criteria and prerequisite to achieving better alloying results during LSA. Appropriate selection and control (optimization) of processing parameters such as scan speed and the laser power can reduce to a large extent the microstructural inhomogeneities which invariably affect corrosion properties. There could possibly be some tiny holes in the coatings due to imperfect contact of Al powder with the substrate in some local areas. Pitting corrosion should preferentially initiate at these defects (tiny holes and very thin areas) in the alloyed layer. For some alloyed layers if it is broken somewhere, then severe corrosion of the substrate will occur in that location, but the reinforcement-matrix interfaces of the alloyed sample in this work were clean, thereby resulting in a stronger particle-matrix bonding. The structure and chemical behaviour of Al-based matrix reinforced with (*Cu + Mo*) alloying elements are well established. If tiny holes exist in the alloyed zone it is rather minimal and invisible.

However, minimal selective corrosion attack was observed to take place in the laser alloyed sample. The surface morphology of the laser treated layer after polarization (Figure 8) revealed that some tiny pits were located in the regions between the unreacted *Mo*, Al-matrix and Al_5Mo phase. Once precipitates are formed in aluminium matrices, galvanic microcells are produced between these precipitates and the aluminium matrix due to differences in potential, resulting in selective attack. The surface morphology of polarized surface did show minimal selective dissolution at these interfaces. Generally, the Al-Cu-Mo surface did not dissociate and it is more protective against corrosion attack than the unreinforced alloy resulting in more positive pitting potential as recorded in Table 2. The high corrosion resistance displayed by this sample can be attributed to the protective oxide films formed on the sample after immersion in the chloride solution. The corrosion products formed on the alloyed sample were analyzed using the Raman spectrometry.

The Raman spectrum of the corrosion products formed on the surface of alloyed sample after corrosion test was observed within the 100-1500 cm^{-1} spectrum range as shown in Figure 8. Raman bands typical for CuO around 300 and 600 cm^{-1} can be observed but with weak intensities [l]. The bands observed at 340 cm^{-1} and 834 cm^{-1} respectively correspond to Al_2O_3 and MoO_4 [j]. The band at 626 cm^{-1} is typically observed for Cu_2O [k]. As can be seen from Figure 8, the intensities of CuO peaks are relatively weak compared to Cu_2O intensity. From the relative intensities, one can conclude that the relative concentration of Cu_2O is significantly higher on the sample's surface.

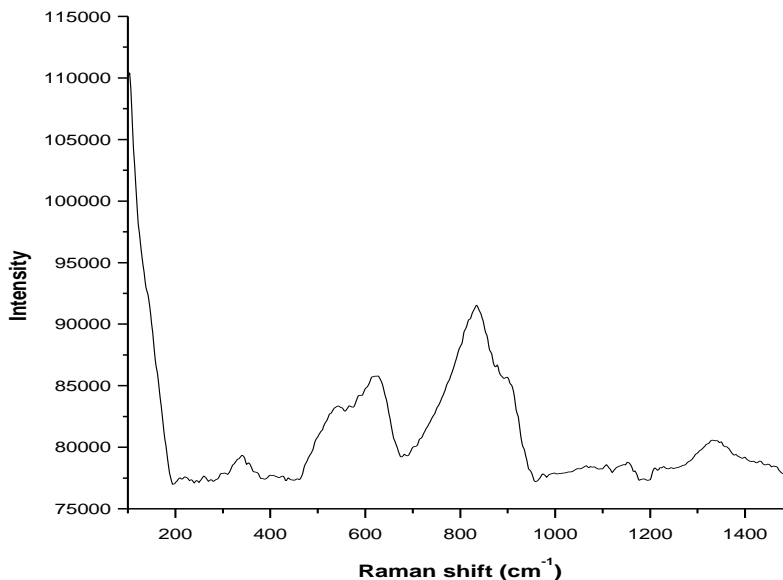


Figure 8. Raman spectrum of *Al-Cu-Mo* sample after electrochemical test in 3.65 % *NaCl*

Figure 9 shows the open circuit potential versus the time curve of the samples. The potential value for alloyed sample was noticed to decrease initially with increase in time. This behaviour suggested that there was a breakdown in the film on its surface at the initial stage, followed by the formation of a new passive film thereafter. The potential values of the alloyed sample remained stable after this behaviour. The alloyed sample displayed a unique behaviour similar to its behaviour in the polarization test. Figure 9 shows that the alloyed sample displayed stable corrosion products throughout the test; this behaviour is an indication of why it exhibited the best corrosion resistance behaviour in the chloride solution.

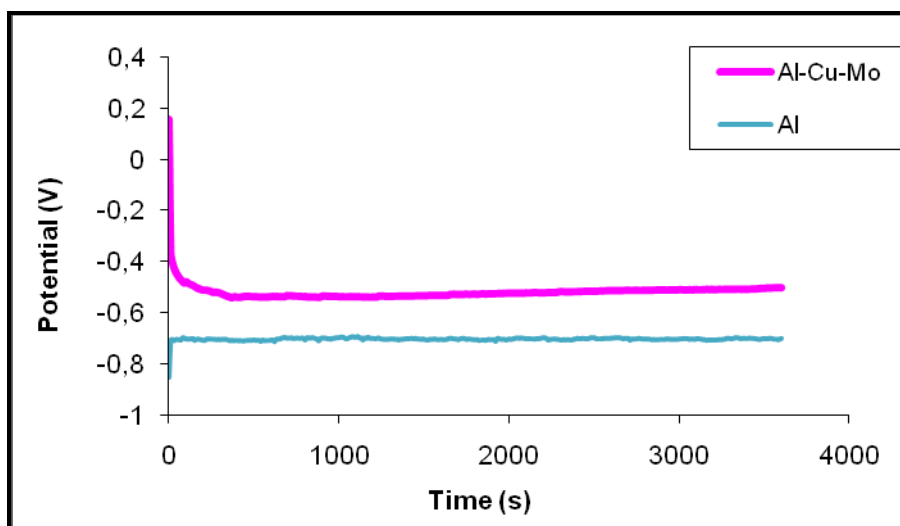


Figure 9. Open circuit potential curve of the *Al-Cu-Mo* sample and as-received *Al*

4. CONCLUSION

Successful fabrication and optimization of a highly corrosion resistant Al/(Cu + Mo) alloyed layer was achieved through laser surface alloying. The addition of 50% copper and 50% molybdenum had a significant positive influence on the corrosion resistance of aluminium. This behaviour can be attributed to the following:

- The microstructure evolved after alloying of the sample: this consisted of a continuous network of Al₂Cu precipitates which is the initial phase, on top of the initial phase are the Al₅Mo intermetallic precipitates and eutectics of (α -Al + Al₂Cu) and (α -Al + Al₅Mo). Grain size refinement was achieved because of the effect of the laser beam.
- Large increase in the corrosion and pitting potentials of the alloyed sample.
- Increase in the polarization resistance by about three orders of magnitude.
- Decrease in the values of corrosion current density and corrosion current by about six orders and seven orders of magnitude respectively.
- Significant decrease of the rate of corrosion was also obtained.
- Higher region of passivity was attained as compared with the pure AA1200. The alloying elements favour the formation of stable protective oxide films that resisted corrosion attack.

ACKNOWLEDGEMENT

The authors would like to thank Tshwane University of Technology (TUT) for financial contributions and CSIR (NLC) for making available lasers and materials for this work.

References

1. H.C. Man, S. Zhang, T.M. Yue and F.T. Cheng, *Surface and Coatings Technology*, 148 (2001) 136-142.
2. A. Almeida, M. Anjos, R. Vilar, R. Li, M.G.S. Ferreira, W.M. Steen and K.G. Watkins, *Surface and Coatings Technology*, 70 (1995) 221-229.
3. K.G. Watkins, Z. Lui, M. McMahan, R. Vilar and M.G.S. Ferreira, *Materials Science and Engineering A252* (1998) 292-300.
4. W.L. Xu, T.M. Yue and H.C. Man, *Journal of Materials Science*, 43 (2008) 942-951.
5. P.H. Chong, H.C. Man and T.M. Yue, *Surface and Coatings Technology*, 154 (2002) 268-275.
6. I. Son, H. Nakano, S. Oue, S. Kobayashi, H. Fukushima and Z. Horita, *Trans. Nonferrous Met. Soc. China*, 19 (2009) 904-908.
7. W.R. Osório, L.C. Peixoto, L.R. Garcia and A. Garcia, *Acta Metall. Sin. (Engl. Lett.)*, 22 (2009) 241-246.
8. A.E. Al-Rawajfeh, S.M.A Qawabah, *Emirates Journal for Engineering Research*, 14 (2009) 47-52.
9. D. Nickel, G. Alisch, H. Podlesak, M. Hockauf, G. Fritsche and T. Lampke, *Rev. Adv. Mater. Sci.* 25 (2010) 261-269.
10. A. Guevara-Lara, R. Bacaud and M. Vrinat, *Applied Catalysis*, 328 (2007) 99-108.
11. M. Kilo, C. Schild, A. Wokaun and A. Baiker, *Journal of Chemical Society Faraday Transactions*, 88 (1992) 1453-1501.
12. J.F. Xu, W. Ji, Z.X. Shen, W.S. Li, S.H. Tang, X.R. Ye, D.Z. Jia and X.Q. Xin, *Journal of Raman Spectroscopy*, 30 (1999) 413-415.
13. Princeton Applied Research, Electrochemical Instruments Division 1-12